Mon. Not. R. Astron. Soc. **000**, 000–000 (0000) Printed 5 March 2001 (MN LATEX style file v1.4)

Indirect imaging of the accretion stream in eclipsing polars - III. HU Aquarii low state

M. K. Harrop-Allin, S. B. Potter* and Mark Cropper
Mullard Space Science Laboratory, University College London, Holmbury St. Mary, Dorking, Surrey RH5 6NT

Received:

ABSTRACT
We apply our technique for indirect imaging of the accretion stream to the polar HU Aqr, using eclipse profiles observed when the system was in a low accretion state. The eclipse profile is different from that in the high state, and more variable from cycle to cycle. We find that the stream maps are brightest near the white dwarf and there is no significant brightening in the threading region. In the low state the stream threads onto the magnetic field closer to the L_1 point than in the high state, with a footpoint of the accreting field line at high latitude. We then produce maps of the accretion region from polarimetry using Stokes imaging. These show that the majority of the accretion occurs near the equator. The difference between the maps may be explained if most of the stream material is not emitting significantly in the low state. If so, neither the stream eclipse mapping nor Doppler tomography techniques will trace the bulk of the accretion flow between the two stars.

Key words: accretion, accretion discs – binaries: eclipsing – cataclysmic variables – stars: individual: HU Aqr

1 INTRODUCTION

We continue our investigation of the accretion stream in polars (Harrop-Allin, Hakala & Cropper 1998 – Paper 1, Harrop-Allin et al. 1999 – Paper 2) with a study of the eclipsing system HU Aqr in a low accretion state, based on simultaneous high speed optical photometry and polarimetry. Observational constraints on the way the accretion stream threads onto the magnetic field are important because the threading process is highly non-linear and therefore difficult theoretically, and because the threading process is itself interesting. The extent of the threading region, and the amount of material resident there (Liebert & Stockman 1985) needs quantification. Moreover, because the material subsequently follows trajectories along field lines, the shape and structure of the accretion regions on the white dwarf are set from this point on. Reviews on polars can be found in Cropper (1990) and Warner (1995), and other investigations into the accretion streams using Doppler tomography and eclipse mapping can be found, for example, in Schwope et al. (1999), Vrielmann & Schwope (1999), Kube, Gaensicke & Beuermann (2000), Heerlein, Horne & Schwope (1999) and Schwope, Mantel & Horne (1997).

We apply the stream imaging method described in Paper 1 to eclipse light curves to construct images of the accretion stream. We then use the polarization curves to construct images of the accretion region on the white dwarf using another genetic algorithm-based optimization method, Stokes imaging (Potter et al. 1998). Unlike previous techniques, this method does not assume *a priori* the shape of the cyclotron-emitting regions on the white dwarf in order to construct model polarization and intensity light curves.

Because the accretion region lies at the footpoints of the field lines in the threading region, the two imaging methods describeed above should produce compatible results if the assumptions for both methods are valid. The results may be difficult to interpret if the magnetic field in the threading region is distorted substantially by the incoming plasma, or if the field is dominated by higher order multipoles near to the white dwarf surface. Although the two imaging methods are not completely consistent (the stream imaging technique assumes that the accretion region is not extended, for example), they may be expected to give broadly compatible results. The two methods have several assumptions and parameters in common: both methods assume that the white dwarf's magnetic field is an inclined dipole, and both methods derive approximate values for the angle between the white dwarf spin axis and magnetic pole β and the longitude ζ of the magnetic pole with respect to the line of centres of the two stars. Our simultaneous photometry and polarimetry thus provides an opportunity to use both Stokes imaging and the stream imaging technique to connect the

* Current address: South African Astronomical Observatory, PO Box 9, Observatory 7935, South Africa.

properties of the accretion flow to the shape and location of the accretion region on the white dwarf.

2 THE OBSERVATIONS

Simultaneous polarization and intensity observations of HU Aqr were made on October 12, 13 and 14, 1996, using the UCT Polarimeter (Cropper 1985) on the 1.9 m telescope at the Sutherland site of the South African Astronomical Observatory. The polarimeter was used in its simultaneous linear and circular polarimetry and photometry mode. A white light bandpass (3200–9200 Å) defined by the RCA 31034A GaAs photomultiplier was used for all time-series observations. The integration time was 10 s for the high speed photometry and 60 s for the polarimetry. Sky measurements were made every $\sim$ 35 min to correct for the background polarization.

V-band measurements of HU Aqr were obtained for calibration purposes on October 13 and 14. These were compared to the V magnitude of star "C" of Schwope, Thomas & Beuermann (1993) (shown in their figure 1). The mean out-of-eclipse V magnitude of HU Aqr was found to be $V \approx 16.3$ (compare this to the mean out-of-eclipse magnitudes in the high state, where $V \approx 15.0$ – see Paper 2). HU Aqr was less than half as bright in October 1996 as it was in October 1992, when the star is described as being in an "intermediate" state (Schwope et al. 1995). It is thus reasonable to say that the October 1996 observations were made in a "low" accretion state.

The data were phase-folded using the ephemeris of Schwope et al. (1997) and the polarimetry was binned to a phase resolution of $d\phi = 0.02$ for the Stokes imaging procedure. The original resolution of 10 s ($d\phi \approx 0.0013$) of the high speed photometry was retained for the stream imaging technique.

2.1 The light curve

The folded light curve is shown in the top panel of Fig. 1. There are pronounced differences between the high and the low state light curves (for comparison see fig. 1 of Schwope et al. 1997). The high state light curve has a double-peaked shape with two maxima per orbit, while the low state light curve has only one peak per orbit. As a result, the eclipse in the high state occurs near a local minimum of the orbital trend, while the low state eclipse occurs between the orbital maximum (at $\phi \approx 0.80$) and the following local minimum at $\phi \approx 1.45$. Unlike the high state, there is no obvious pre-eclipse absorption dip in the low state optical light curve.

The low state eclipse profiles are similar to those in the high state in that they show a multi-component structure. The ingress and egress of the accretion region on the white dwarf occur at $\phi \approx 0.963$ and $\phi \approx 1.037$ respectively, and the ingress of the accretion stream occurs in the interval $0.96 \lesssim \phi \lesssim 1.00$. The ratio of the stream brightness to the accretion region brightness is 0.19, much smaller than in the high accretion state (see Paper 2). The duration of the stream ingress is more than twice as long as in the high state: $\sim$ 290–410 s as opposed to $\sim$ 125 s. Because the stream is relatively less bright than in the high state, the egress of the stream at $\phi \sim 1.04 - 1.15$ is less prominent.

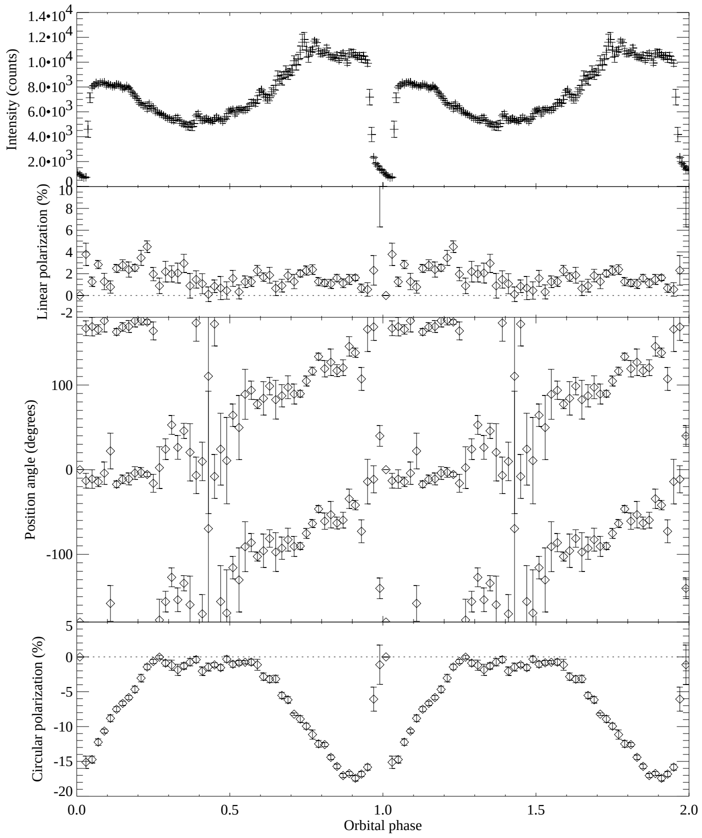

Figure 1. Phase-binned, folded white light photometry and polarization data of HU Aqr for 12, 13 and 14 October 1996, when in the low state.

Four complete eclipses were observed during the three nights of observation (two successive eclipses were acquired on 13 October), corresponding to cycles 16964, 16975, 16976 and 16986 according to the ephemeris of Schwope et al. (1997) – these will be referred to as cycles 1, 2, 3 and 4 for brevity. They are shown in their original 10 s resolution in Fig. 2. Unlike the high state data, the duration of the accretion stream ingress in the low state data is highly variable from cycle to cycle. No two eclipses have the same stream ingress duration: the component changes from $\sim$ 410 s in cycle 1, to $\sim$ 390 s, $\sim$ 270 s and $\sim$ 300 s in cycles 2, 3 and 4 respectively. Note the large change between the two *successive* cycles of 13 October (cycles 2 and 3).

2.2 Polarimetry

The circular and linear polarization curves, and the variation of the position angle of the linear polarization, are shown in the bottom three panels of Fig. 1. The circular polarization curve is roughly sinusoidal and is negative at all phases, reaching -17 per cent at $\phi \approx 0.9$. The shape and phasing of the circular polarization curve is similar to that of Hakala et al. (1993). The linear polarization is significant but low throughout the orbit: most measurements are below 5 per cent. There are no obvious linear polarization peaks during the orbit (the high point at $\phi \approx 0.0$ is not reliable because the system is in mid-eclipse at this phase).

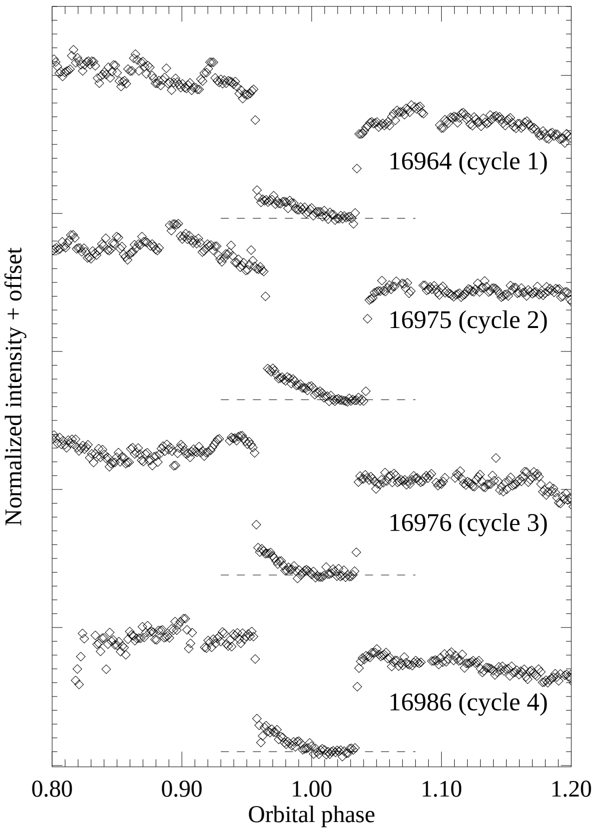

Figure 2. Eclipse profiles of HU Aqr in a low accretion state on 12, 13 and 14 October 1996. Each eclipse is labelled with the corresponding cycle number according to the ephemeris of Schwope et al. (1997). The eclipses of 12 and 13 October have been offset for clarity. The mid-eclipse intensity is shown as a dashed line for each eclipse.

The circular polarization data suggest that the stream accretes onto only one pole, since the excursions in the curve are of only one sign. In this regard, HU Aqr in the low accretion state resembles ST LMi and VV Pup (*cf* Cropper 1990). It is interesting to note, however, that circular polarimetry of HU Aqr in the high state shows both positive and negative excursions (Hakala, unpublished data).

3 INDIRECT IMAGING OF THE ACCRETION STREAM

3.1 Photospheric contributions

Towards the end of the eclipse, the white dwarf primary and all of the accretion stream has been eclipsed. The only source of intensity is the photosphere of the secondary. Its contribution can be seen to be negligible in our passband at this phase in Fig. 1. This can also be inferred from figure 2 of Schwope et al. (1993), especially since this exposure includes part of the eclipse, thus increasing the relative contribution of the secondary to the spectrum. Any variability in the secondary contribution (due to, for example, ellipsoidal variations) will typically be limited to $\lesssim$ 20 per cent of the already negligible level.

Isolating the contribution from the white dwarf can be achieved by noting that its eclipse will last ~ 40 sec. There are no components evident in the eclipse profiles with this timescale: the main feature in the eclipses in Fig. 2 is a sharp drop and rise in brightness on a timescale unresolved in our 10 sec integrations. The size of the corresponding emitting region, and the drop in polarised flux at this phase, indicates that this is the eclipse of the cyclotron emitting region, together with any associated heated region in the white dwarf photosphere. This indicates that the emission from the photosphere as a whole but excluding the heated region does not contribute significantly to the intensity. Again this is corroborated by the extrapolation of modelled UV HST data into the V band by Gänsicke (1999), where the non-heated photosphere can be calculated to contribute at most 15 per cent of the flux.

3.2 Removal of the orbital trend

The decreasing trend (Fig. 3) in the intensity data will lead to systematic errors in the stream maps if no correction is made for the changing brightness of the cyclotron emitting region.

The long stream ingress after the spot has been eclipsed (and when there are no additional sources of emission) requires the stream eclipse to start at phase $\phi \sim 0.9$ and to end at phase $\phi \sim 1.15$. (This is true for both the ζ and L1 configurations we consider in the next section.) The relatively clear features in the light curve evident at these phases in Fig. 3 can therefore be identified with the stream eclipse, with a good degree of confidence. As there is no evidence that subtraction of any more complicated trend over this phase range is justified (this is supported by the cyclotron modelling below), we have adopted the simplest approach of removing a linear trend between $\phi = 0.9$ and 1.15. We have smoothed the intensity values with $\phi \lesssim 0.90$ and $\phi \gtrsim 1.15$ using a running mean over 20 points and then interpolated between the two intervals of smoothed data using a linear trend. This is then subtracted from the original light curve (excluding the range $0.956 \lesssim \phi \lesssim 1.036$, where the cyclotron region is not visible). This procedure is illustrated in Fig. 3.

3.3 Details of the model

As described in Paper 1, several decisions have to be made before the imaging procedure can be applied — these include choosing values for the fixed parameters (the white dwarf mass M_1, the mass ratio q, inclination i, the threading radius after which the ballistic trajectory becomes a magnetically dominated one R_μ and the colatitude and longitude of the magnetic pole β and ζ), choosing whether to use a one-footpoint or a two-footpoint geometry, and deciding whether to include projection factors in the model calculation to account for optical depth effects. The modelling is strongly sensitive to some of these parameters (for example i) but less so for others (such as β and ζ).

The simultaneous circular polarimetry indicates one-pole accretion, implying that the one-footpoint geometry is the correct choice. The two-footpoint geometry may be more appropriate, however, if luminous threaded material accumulates in the magnetosphere on field lines whose footpoints lie near the second pole, without proceeding to the

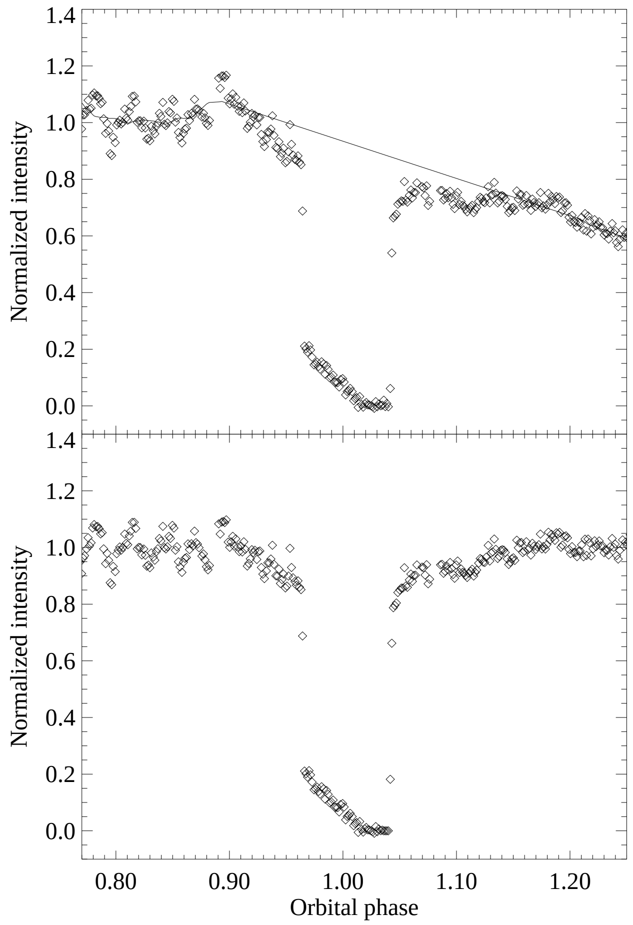

Figure 3. Subtracting the orbital trend in the low accretion state photometry of HU Aqr. The upper panel shows the light curve surrounding the eclipse (the eclipse shown is that of cycle 2); superimposed is the spline fit that is used to approximate the orbital trend during the eclipse. The lower panel shows the results of the subtraction procedure (see text for details).

white dwarf surface. This stream plasma could contribute to the stream brightness without adding appreciably to the cyclotron flux. For the purposes of this investigation, however, we have opted for the more immediately obvious single footpoint model.

In the high state eclipse profiles, projection factors were included in the model because the stream in the high state is (at least partially) optically thick (see Paper 2): this can be seen by the presence of the pre-eclipse absorption dip. In the low state there is not as much direct evidence that optical depth effects are important: for instance, there is no pre-eclipse absorption dip in the optical light curve. This implies that the parts of the stream that cut the line of sight are not significantly optically thick. However, this does not mean that the entire stream has negligible optical depth: projection effects may be necessary in other parts of the stream. We therefore decided to include projection effects in the stream.

Uncertainties were assigned to the light curves in the following way (this procedure is similar to that in Paper 2). Points with $\phi < 0.89$ or $\phi > 1.13$ were assigned large errors, since the accretion stream is fully visible for these phases, and thus no information is available from the eclipses. The narrow phase ranges during which the accretion region is eclipsed ($0.956 \lesssim \phi \lesssim 0.958$) and coming into view ($1.034 \lesssim \phi \lesssim 1.036$) were also assigned large errors: the model assumes that the accretion region is a dimensionless point, whereas in reality the accretion regions are extended and their eclipses are not instantaneous. The uncertainties used for the remainder of the eclipse profile were assumed to be equal to the Poisson uncertainties ($\sqrt{n}$, where n is the number of counts in a given integration).

The main difference between the high state and the low state eclipse profiles is the remarkably long stream ingress, which is more than twice as long in the low state than in the high state. This implies that the stream travels further away from the line of centres between the component stars and/or further out of the orbital plane before heading towards the white dwarf. The stream models can produce the long stream ingress in only two ways. In the first configuration we follow the treatment in Paper 2, but the values for ζ and R_μ have to be larger: $\zeta \sim 90^\circ$ and $R_\mu \sim 0.50\,a$ (where a is the binary separation). These parameters produce a trajectory where the stream becomes coupled to a magnetic field line close to the secondary. The field line lifts the stream far out of the orbital plane. The long stream ingress component is thus produced by the ingress of the *magnetically-channeled* part of the stream (this configuration is referred to as the "ζ configuration" for brevity).

The change in ζ from $\sim 10^\circ$ in the high state (Paper 2) to $\sim 90^\circ$ in the low state between high and low states is large (although not impossible: the timescale for oscillations of the magnetic pole is ~ 20 years for HU Aqr, Campbell & Schwope, 1999). For this reason we have explored whether there are other ways of producing the long stream eclipse, while maintaining a relatively unchanged ζ. This requires the stream to move further from the line of centres than would be reached using the standard ballistic trajectory (Lubow & Shu 1975). The only way to achieve this is to impart an additional non-thermal velocity to the material leaving the L1 point, so that, in this second configuration, the ballistic stream is made to leave the L1 point at an angle greater than the usual $\sim 20^\circ$ ($R_\mu \approx 0.30$). The long stream ingress is then produced by the ingress of the *ballistic* stream. This configuration is referred to as the "L1 configuration". The two models are illustrated in Fig. 4.

In the L1 configuration, the large angle between the ballistic stream and the line of centres (approximately 32°) is achieved by increasing the velocities with which the stream leaves the L1 point from $320\,\mathrm{km\,s^{-1}}$ to $450\,\mathrm{km\,s^{-1}}$ in the y-direction (in the direction of the rotation of the secondary) and from $10\,\mathrm{km\,s^{-1}}$ to $100\,\mathrm{km\,s^{-1}}$ in the negative x-direction (along the line of centres towards the white dwarf). This might be caused by the same mechanism that has been proposed to cause the low states in mCVs. Livio & Pringle (1994) invoke star spots on the secondary in the region of the L1 point to explain the low states of VY Scl stars. King & Cannizzo (1998) show that the low states of polars are also consistent with this model. A star spot could inhibit the flow of material through the L1 point by reducing the local scale height in the secondary's atmosphere. For the magnetic field to affect significantly the mass transfer rate, Livio & Pringle (1994) estimate that the magnetic pressure in the star spot would have to be comparable to the gas

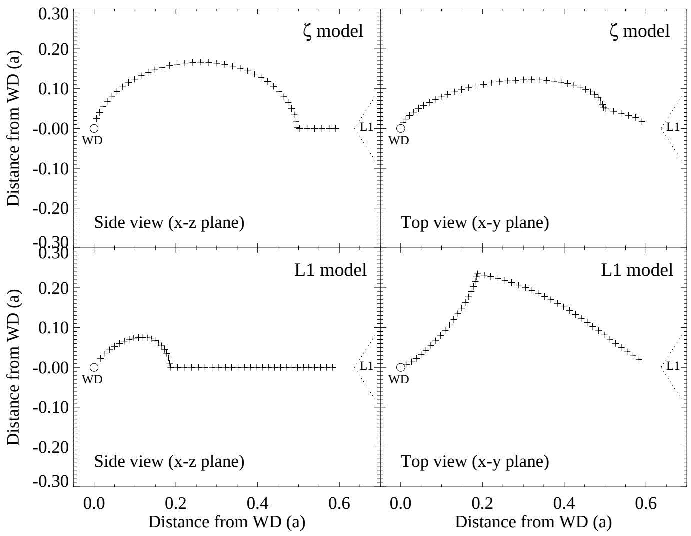

Figure 4. The two stream configurations used to model the low state eclipse profiles (the examples shown are those constructed to model the eclipse of cycle 4). The upper panels show the ζ configuration and the lower panels show the L1 configuration (see text for details). The streams are shown projected onto the x–z plane (side view) on the left, and projected onto the x–y plane (viewed from above the orbital plane) on the right.

pressure there. The increased magnetic pressure in the star spot at the L1 point could also modify the initial trajectory of the ballistic stream as it leaves the secondary.

3.4 Stream imaging results

3.4.1 ζ configuration

Fig. 5 shows the model fits and the corresponding stream images for the four low state eclipses using the ζ configuration. The stream images are shown as projections onto the (x–z) plane (i.e. looking along the plane of the orbit). The dipole offset and inclination are $\beta = 25°$and $i = 85°$ (Paper 2). A value of $R_\mu = 0.50$ was found to be acceptable in all four fits. The change between the long stream ingress components (~ 400 s) of cycles 1 and 2, and the much shorter stream ingresses of cycles 3 and 4 (~ 290 s) is achieved by decreasing the value of ζ from 90° for the first two eclipses, to 80° for the last two. The fits have $\chi^2/N \approx 3$.

All four cycles have streams which brighten towards the white dwarf; with the exception of cycle 1, the stream is brightest *at* the white dwarf. The stream image for cycle 1 has a localized bright region on the magnetically-channeled part of the stream; the other cycles have more slowly-varying brightness distributions along the field line. The first two cycles have bright ballistic streams; in cycle 1 the ballistic stream brightens as it approaches R_μ and in cycle 2 the ballistic stream fades as it approaches R_μ. The last two cycles have fainter ballistic streams, and almost all the stream emission occurs along the magnetically-channeled part of the stream.

The accretion spot (the footpoint of the accreting field line) predicted by the model for cycles 1 and 2 is at a latitude of 12° and a longitude of 30°, where latitude is measured from the spin axis of the white dwarf towards the orbital plane and longitude is measured from the line of centres in the direction of the motion of the secondary star. The spot position for cycles 3 and 4 is slightly different: the latitude is 21° and the longitude is 30°.

3.4.2 L1 configuration

Fig. 6 shows the model fits and the corresponding stream images for the four low state eclipses using the L1 configuration. This time the stream images are shown as projections onto the (x–y) plane (i.e. looking down onto the orbital plane) for clarity. As before, the dipole offset is $\beta = 25°$ in all four fits. The duration of the stream ingress is controlled in these models by the value of R_μ: the longer the stream ingress, the smaller the value of R_μ required. The first two eclipses are modelled using $R_\mu = 0.28\,a$, while cycle 3 has $R_\mu = 0.34\,a$ and cycle 4 has $R_\mu = 0.30\,a$. The fits have $\chi^2/N \approx 3$.

The four images have a varied appearance: the ballistic stream brightens towards R_μ (cycles 3 and 4), fades towards R_μ (cycle 2) or stays roughly constant until R_μ (cycle 1), while the magnetically-channeled stream brightens towards the white dwarf (cycles 1, 2 and 4) or stays roughly the same (cycle 3). The cycle-to-cycle changes in the stream images are much larger in the low state than in the high state (this is the case for both the ζ and the L1 configurations).

The footpoint of the accreting field line in cycles 1 and 2 occurs at a latitude of 69° and a longitude of 30°, while in cycles 3 and 4 the footpoint is at 78° latitude and 33° longitude.

4 STOKES IMAGING OF THE ACCRETION REGION

Further information regarding the nature of the accretion process in HU Aqr can be found in the polarimetry obtained simultaneously with the high speed photometry. We model the polarimetry using the Stokes imaging procedure (Potter et al. 1998) to deduce the structure and location of the accretion region on the white dwarf. We then compare the structures on the white dwarf to the results of the stream imaging technique in order to link the accretion flow between the two stars to the accretion structures on the primary.

4.1 Description of the method

The Stokes imaging procedure produces images of the accretion region on the white dwarf by optimizing model fits to intensity and polarization light curves. The models are based on the cyclotron emission calculations of Wickramasinghe & Meggitt (1985). Given the viewing angle to any emitting point on the white dwarf, and values for the electron temperature T_e and the optical depth parameter Λ, the Wickramasinghe & Meggitt cyclotron models can be interpolated to give the Stokes parameters (I, Q, U and V) emitted by the point for all cyclotron harmonics.

An extended emission region is constructed using several adjacent emission points. To calculate the model polarization and intensity, the Stokes parameters are calculated

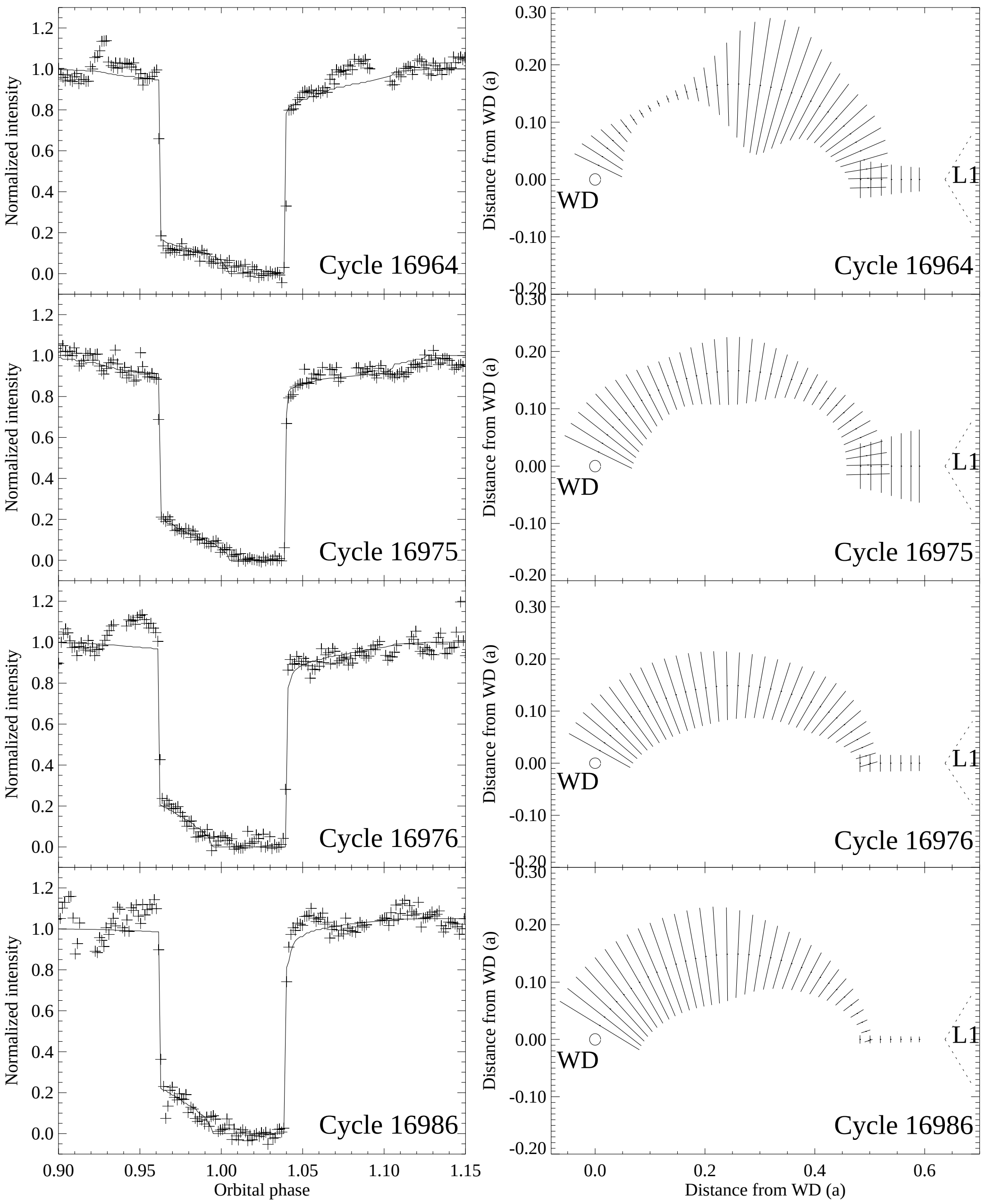

Figure 5. Model eclipse profiles and the corresponding stream images for the low state eclipses using the ζ configuration. The stream images are shown projected onto the $(x$–$z)$ plane (side view). The brightness of each stream emission point is indicated as a line perpendicular to the stream; the length of the line represents the brightness of the point. The white dwarf is shown to scale as a circle (labelled 'WD'), and the secondary is shown (not to scale) to mark the position of the L1 point (labelled 'L1').

for each point in the region and summed to yield values for the intensity, percentage circular and linear polarization and the resulting position angle of the linear polarization. The corresponding light curves are then constructed by viewing the ensemble of points as a function of phase. Radiative transfer through the accretion region is not calculated; as a first order approximation to optical depth effects, a projection term (the cosine of the viewing angle) is included to simulate absorption effects within the extended accretion region (cyclotron emission is optically thick for the lower harmonics). Because the Wickramasinghe & Meggitt (1985) models are for homogeneous plasmas without geometrical structure, the observed polarisations will be lower than calculated, so a constant dilution factor is applied, which, to first order, also takes account of non-cyclotron emission from the system.

Another simplifying assumption used in the Stokes imaging algorithm is that the accretion region has no vertical height above the white dwarf surface. This may be inaccurate because the height of the stand-off shock varies approximately inversely with the density of infalling material. In general, therefore, the rim of the shock (i.e. where the flow

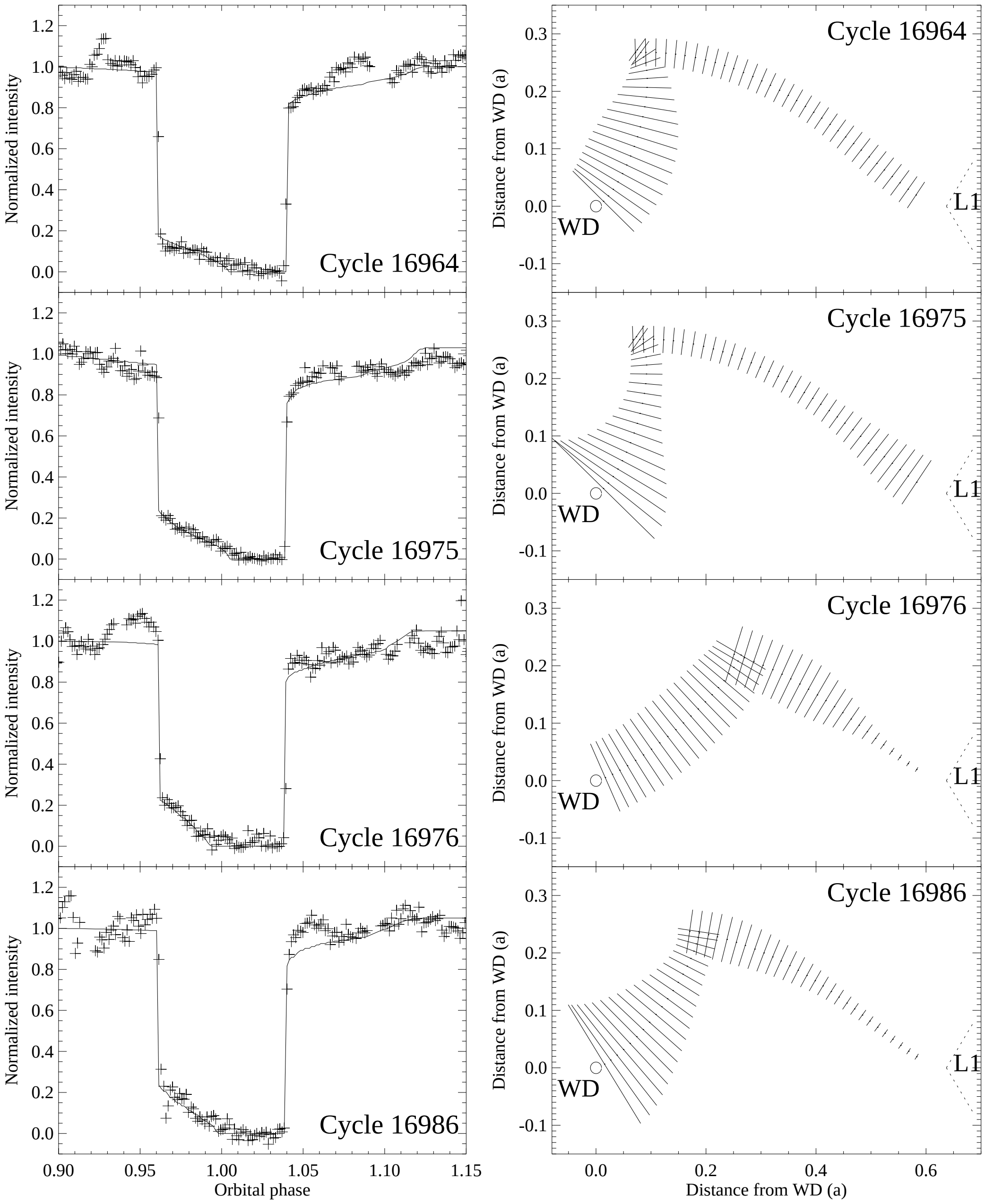

Figure 6. As Fig. 5 but for the L1 configuration. The stream images are shown projected onto the (x–y) plane (looking down onto the orbital plane) for clarity.

is less dense) is expected to rise to a considerable height above the white dwarf surface ($\gtrsim 0.1\,R_1$). Other limitations of the Stokes imaging technique are discussed in Potter et al. (1998).

The surface of the white dwarf was divided into a grid of 1740 points, each corresponding to an area of 6 square degrees in magnetic coordinates. Each emission point on the grid was assigned a value for Λ, and the Stokes parameters are calculated for the emission region for each phase to construct the intensity and polarization light curves as before. A genetic algorithm was used to breed solutions based on their fitness. The fitness function used for Stokes imaging has a similar form to equation (1) in Paper 1, although a Tikhonov regularization term replaces the maximum entropy term. The solution from the genetic algorithm is then refined using Powell's method, as is done in the stream imaging technique. For more details of the method, and tests using synthetic data, see Potter et al. (1998).

4.2 Removing the stream contribution from the light curve

Removing known sources of variable non-cyclotron emission before the Stokes imaging procedure is applied maximises the fidelity of the procedure. The low state eclipse profiles indicate that the accretion stream is a contributor at the

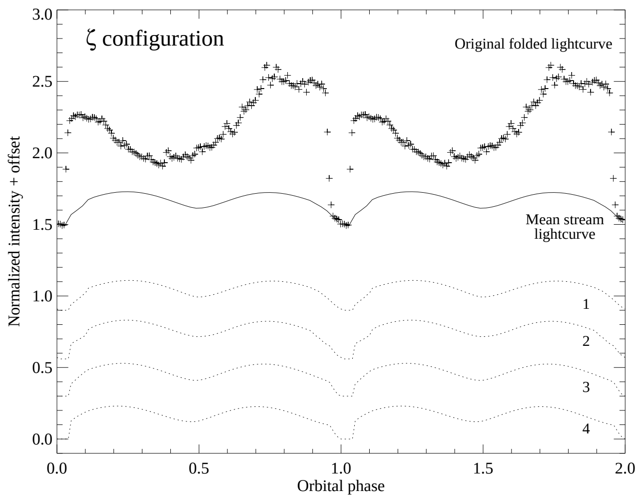

Figure 7. Constructing a mean stream light curve for the ζ configuration stream models. The stream light curves derived from the model streams for each eclipse profile are labelled with the corresponding cycle number. These individual light curves are averaged to obtain the mean stream light curve for the ζ configuration. This is shown superimposed on the original intensity light curve at the top of the figure.

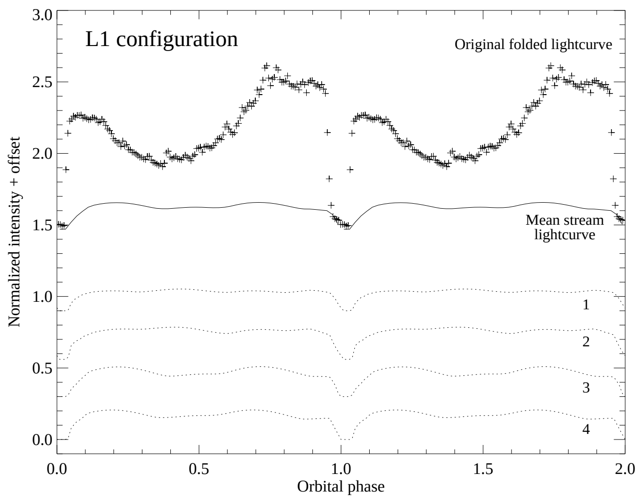

Figure 8. As for Fig. 7, but for the L1 configuration.

$\sim$ 20 per cent level to the overall intensity. This contribution can be removed by using the stream models constructed in section 3.4. Given a model stream, the corresponding stream light curve can be constructed by calculating the model stream at all orbital phases. This stream light curve can then be subtracted from the original intensity light curve to yield a better estimation of the cyclotron emission.

The Stokes imaging procedure is applied to the folded data because the signal-to-noise ratio of the individual intensity and polarization light curves is not sufficiently high to apply the technique to each in turn. A mean stream light curve must therefore be constructed from the individuals stream models for cycles 1–4. This is done by generating the model streams for each individual light curve for the whole orbit, and then calculating the mean light curve. This process is illustrated for each of the two stream configurations in Fig. 7 and Fig. 8.

The stream light curves obtained using the ζ configuration have larger amplitudes of variation than the stream light curves from the L1 configuration. This is because in the ζ configuration, the stream is more aligned with the line of centres, and is therefore seen almost edge-on at $\phi = 0.5$ — in projection, therefore, the stream is fainter at this phase (the stream is almost edge-on also at $\phi = 1.0$, when the eclipse by the secondary occurs). The L1 configuration stream is not as well-aligned with the line of centres, and the corresponding streams do not produce an orbital modulation with as large an amplitude.

We subtracted the mean stream light curve for each of the two configurations from the folded intensity light curve to produce the intensity light curves for the Stokes imaging process.

4.3 Stokes imaging results

4.3.1 ζ configuration

The model fits to the polarization and intensity light curves are shown in Fig. 9. These fits were obtained assuming $i = 85°$ (as for the stream imaging) and $B = 37\,\mathrm{MG}$ (e.g. Glenn et al. 1994; Schwope et al. 1997). The dipole field has $\beta = 14°$ and $\zeta = 72°$. The gross features of the data are predicted by the model, but some of the details are not well-reproduced. The model underestimates the intensity at in the phase range $0.08 \lesssim \phi \lesssim 0.60$ and overestimates the magnitude of the circular polarization in the phase range $0.9 \lesssim \phi \lesssim 1.2$. The model also underestimates the linear polarization level in the range $0.15 \lesssim \phi \lesssim 0.40$.

The accretion region predicted by the model is shown in Fig. 10 as a grey-scale image. This figure is an equal-areas projection of the white dwarf in spin coordinates.

The Stokes imaging algorithm has predicted a large, broken accretion region near the equator of the white dwarf (i.e. near the orbital plane) composed of two main regions, one extending from a latitude $\sim 50°$ to $\sim 90°$ and longitude $\sim 15°$ to $\sim 45°$, and the other extending from a latitude $\sim 60°$ to $\sim 90°$ and a longitude of $\sim 65°$ to $\sim 85°$. A third smaller and fainter region occurs at latitude $\sim 25°$ and longitude $\sim 100°$.

4.3.2 L1 configuration

The model fits for the L1 configuration are shown in Fig. 11. The dipole parameters for this fit are $\beta = 22°$ and $\zeta = 108°$. As for the ζ configuration model, the inclination and field strength were fixed at 85° and 37 MG respectively. The quality of these fits is better than those for the ζ configuration. The phase ranges where the model does not reproduce the data well are similar to the poorly-fit sections of the ζ configuration model. As before, the model underestimates the intensity in the range $0.08 \lesssim \phi \lesssim 1.6$ and overestimates the magnitude of the circular polarization in the range $0.9 \lesssim \phi \lesssim 1.3$. The percentage linear polarization is underestimated in the range $0.1 \lesssim \phi \lesssim 0.4$.

The image of the accretion region generated by the Stokes imaging procedure is shown in Fig. 12. As in the

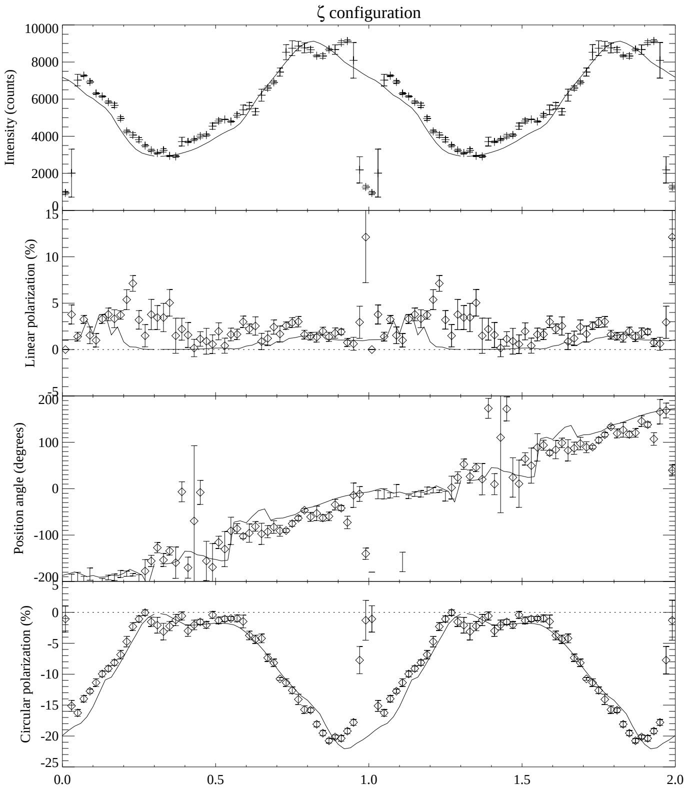

Figure 9. The Stokes imaging model fits to the low state intensity and polarization light curves for the ζ configuration.

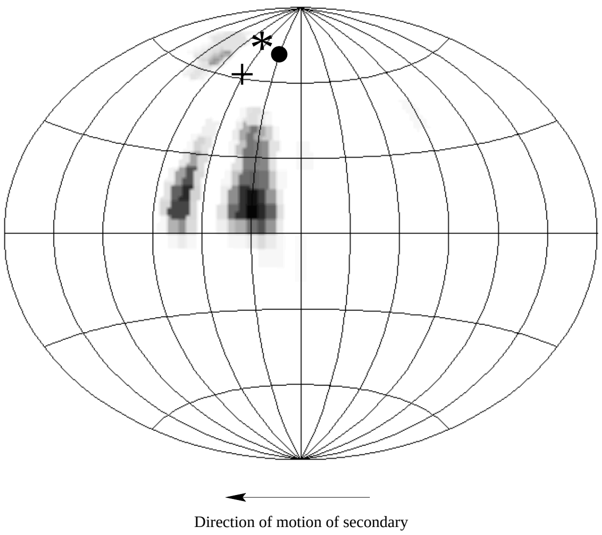

[t]

Figure 10. An equal-areas projection of the white dwarf surface in spin coordinates showing the results of the Stokes imaging method for the ζ configuration. The line of centres defines longitude zero on the primary; this line occurs at the centre of the diagram and longitude is measured from this line in the direction of motion of the secondary. Latitude is measured from 0° at the spin pole above the orbital plane (at the top of the diagram). The lines of latitude and longitude indicated are 30° apart. The position of the magnetic pole predicted by the Stokes imaging method is shown as an asterisk. For comparison, the magnetic pole predicted by the stream imaging method is shown as a plus sign, and the average position of the footpoints of the field lines used in the stream imaging method is shown as a filled circle.

ζ configuration, the accretion region is broken into three regions, with most of the emission concentrated in two of the three regions. One of the bright regions extends from a latitude of $\sim 35°$ to $\sim 95°$ and a longitude of $0°$ to $\sim 50°$, and the other is located between $60° - 90°$ in latitude and $55° - 90°$ in longitude. The third region is much fainter and (as before) occurs closer to the spin axis of the white dwarf and closer to the magnetic pole than the two brighter regions, at latitude $\sim 35°$ and longitude $\sim 95°$. The shapes and locations of the accretion regions for the L1 model are very similar to those for the ζ model.

5 DISCUSSION

5.1 Photometry and stream imaging results

In both stream configurations, the fits to the low state eclipse profiles of HU Aqr are not as good as the fits to the high state data in Paper 2: the high state fits have $\chi^2/N \approx 1$ while the low state fits have $\chi^2 \approx 3$. This suggests that the simple trajectory assumed for the stream is not as good an approximation in the low state as in the high state. The low state stream might be expected to deviate more from the simple model, if the stream is less dense. The stream material may be threaded along the length of the ballistic stream, instead of the bulk of the stream threading near R_μ. The absence of a pre-eclipse absorption dip in the low state light curves may also suggest that the accreting material is more spread out in the magnetosphere: there is no collimated portion of the stream on the same side of the orbital plane as the observer that is sufficiently dense to produce an absorption dip (the alternative explanation for the absence of a dip, viz. that the stream is accreting onto the lower pole, is ruled out by the Stokes imaging results).

The generally larger values of R_μ in the low state imply that the stream couples to the magnetic field further from the white dwarf than in the high state. In the ζ configuration, in particular, the values of R_μ are very large ($R_\mu = 0.50$). The mass transfer rate in the stream can be estimated by following the approach in Paper 2. Assuming a stream radius (in units of 10^9 cm) $\sigma_9 = 3$ as in the high state (since there is no absorption dip in the low state to constrain this value), $M_1 = 0.9$, $B = 37\,MG$ and $q = 0.25$, the mass transfer rate is in the range $0.2 - 2.8 \times 10^{16}\,\mathrm{g\,s^{-1}}$. This is more than an order of magnitude below the values obtained for the high state (Paper 2). The main uncertainty in this calculation is the radius σ_9 of the stream, since $\dot{M} \propto \sigma^3$.

5.2 Which is the better model of the low state accretion stream?

As was the case with the two-footpoint vs. the one-footpoint geometry models for the high state data (Paper 2), it is difficult to distinguish between the two low state stream configurations on statistical grounds. However, the plausibility of the two models can be checked using other observations of HU Aqr in low accretion states. The main difference between the ζ and the L1 configurations is the angle between

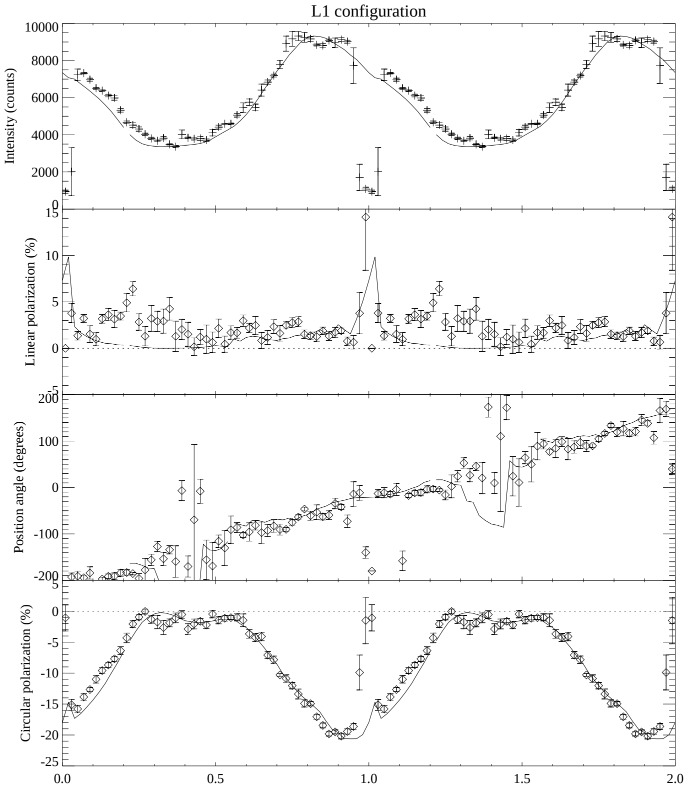

Figure 11. As for Fig. 9, but for the L1 configuration.

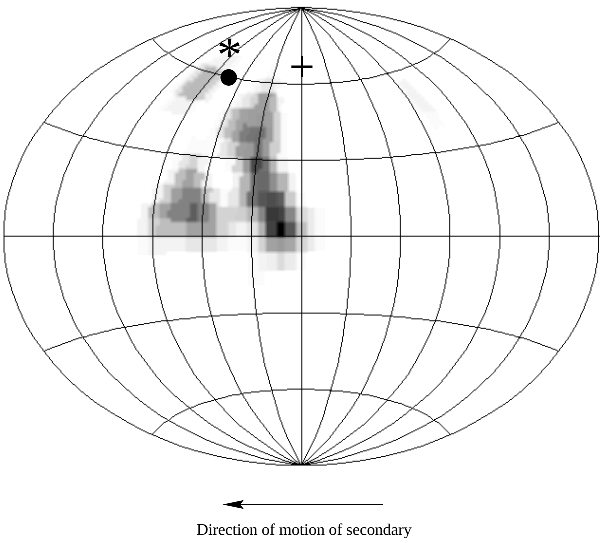

Figure 12. As Fig. 10, but for the L1 configuration.

the magnetically-channeled part of stream and line of centres. This angle should coincide with the phase at which the absorption dip occurs (see Paper 2).

In the low state, although there is no absorption dip in the optical, there *is* an absorption dip in the soft X-rays. In a sequence of *ROSAT* PSPC and HRI light curves of HU Aqr obtained in 'reduced' accretion states from April 1994 to November 1996, Schwope et al. (1998) observe that the pre-eclipse absorption dip approaches the eclipse. During April 1994 and November 1995, the absorption dip and the eclipse appear as separate structures, while in April 1996 and November 1996 the structures are merged. The absorption dip (or the merged dip/eclipse feature) begins at $\phi \approx 0.885$ in April 1994 and at $\phi \approx 0.937$ in November 1996, implying an angle between the line of centres and the magnetically-channeled part of the stream in the range $23°$–$42°$. The range of angles in the stream images for the L1 configuration (see Fig. 6) is $41°$–$71°$. Since these two ranges barely overlap, it might be concluded that the L1 configuration is less plausible than the ζ configuration. This argument is not completely secure, however, because of the high degree of variability of the stream geometry observed in the low state, and the non-simultaneity of the X-ray observations.

5.3 Stokes imaging results

The shapes and locations of the accretion regions (shown in Figs. 10 and 12) are similar for both configurations. This is expected, since the two emission distributions produce similar polarization and intensity light curves. The longitudes of the magnetic poles differ by $36°$, but at these latitudes, the angular displacement between the two poles is only $15°$. The only difference between the input data for the ζ and the L1 configurations is the intensity light curve: the polarization curves for both configurations are identical. The results of the Stokes imaging process are thus sensitive to slight changes in the intensity light curve.

The shapes and locations of the emission regions on the white dwarf are a direct result of how and where the accretion flow threads onto the magnetic field. Material that is diverted from its ballistic trajectory soon after leaving the secondary will accrete close to the magnetic pole, while material that threads closer to the white dwarf will accrete further from the pole. Looking at Figs 10 and 12, the faint region near the magnetic pole could be the accretion region of material that threads far from the white dwarf, while the bright regions nearer the equator might result from material that travels much closer to the white dwarf before being threaded. Since the regions further from the magnetic pole are much brighter than the region near the pole, this suggests that the bulk of the flow penetrates more deeply into the magnetosphere before coupling to the field.

The locations of the emission regions are not, however, consistent with a rigid dipolar magnetic field and a straightforward accretion geometry. In the conventional scenario, material that is threaded soon after leaving the secondary should accrete near the line of centres between the two stars. More dense material, which takes longer to be penetrated by the field, will travel further along its ballistic trajectory and closer to the white dwarf before being threaded. This material would thus accrete further from the line of centres. The emission regions on the white dwarf that are closer to the line of centres should thus also be closer to the magnetic pole, while the emission regions far from the pole should be further from the line of centres. This is clearly not the case in Figs 10 and 12, where the emission region closest to the magnetic pole is the furthest from the line of centres.

It is therefore likely that the accretion geometry in the low accretion state is quite complex. The magnetic field could be distorted so that the threading region is azimuthally extended — this would enable material to thread onto field lines with footpoints closer to the line of centres, even though the threading occurs close to the white dwarf. Another possibility is that the assumption of a dipolar field close to the white dwarf is incorrect, and that the field is dominated by higher-order multipoles near the surface.

5.4 Comparison of results from the two imaging methods

Figs 10 and 12 show the locations of the magnetic poles and accretion spots as predicted by the stream imaging models. The magnetic poles for the two imaging methods are very close in the case of the ζ model, but are separated by $\sim 90^\circ$ in longitude in the L1 model (however, at these high latitudes, the physical distance between these estimates for the position of the pole is not large). This provides additional support for the ζ model. On the other hand, the Stokes imaging fits are better for the L1 model. Ultimately, we are unable to conclude from the evidence available to us which of the two stream-modelling configurations is more appropriate.

We now consider the location of the accretion region. Both the L1 and ζ models show acceptable agreement in longitude between the accreting field lines (the solid dots in Figs 10 and 12) and the accretion region from the Stokes imaging. However, the agreement in latitude is poorer, with the Stokes imaging predicting the main region at significantly lower latitude. This lower latitude is reasonably secure, given simple arguments from the polarimetry: were the main region to be at higher latitude, the position angle would exhibit a wavelike variation. On the other hand, the long duration of the stream eclipse is incompatible with such an equatorial accretion region.

We have considered in the previous section several possible contributors to this disagreement, which centre on the appropriateness of the assumptions behind the modelling process. Alternatively, we may take the broad results from the two techniques at face value. This would imply that the material accreting near the equator in the Stokes imaging maps may be relatively dense, non-luminous and therefore invisible until it encounters the accretion shock on the white dwarf. Unless this material occults an emission source (and it probably wouldn't for the low latitude accretion in the Stokes imaging maps), it would not be evident in the eclipse profiles. These would pick up only that material in the stream which is luminous, accreting (in this case) at higher latitudes. The effect may be strongest when the photoionising flux from the accretion region is less, as in the low state. This would render the stream relatively less luminous than in the high state, as was noted in section 2.1. (A parallel relative decrease in stream brightness in lower states was found in the similar system UZ For by Perryman et al (2001).) The problem may however persist even in higher states if denser or shielded parts of the stream remain essentially dark. The implication is that until the physical processes responsible for both continuum and line emission in the stream are more fully understood (Harrop-Allin 1999), neither Doppler tomography (which depends on the line emitting material) nor stream eclipse mapping may locate the bulk of the material in the accretion stream. This material will be seen only in absorption, for which new techniques will be required.

ACKNOWLEDGEMENTS

MKHA acknowledges funding support from the Graduate School, University College London (Graduate Schools Research Scholarship), the Committeee of Vice Chancellors and Principals of UK Universities (Overseas Research Student Award) and the University of Cape Town (Max & Lillie Sonnenberg Scholarship). MC is grateful to the Director at SAAO for the generous allocation of telescope time, and to Gavin Ramsay for his comments and enthusiasm for seeing this paper published.

REFERENCES

Campbell C., Schwope, A., 1999, A&A, 342, 132
Cropper M., 1985, MNRAS, 212, 719
Cropper M., 1990, SSRv, 54, 195
Gänsicke B. T., 1999, in Hellier, C., Mukai, K., eds, ASP Conf. Ser. 157, Proc Annapolis Workshop on Magnetic Cataclysmic Variables, Astron. Soc. Pac., San Francisco, p. 261
Glenn J., Howell S. B., Schmidt G. D., Liebert J., Grauer A. D., Wagner R. M., 1994, ApJ, 424, 967
Hakala P. J., Watson M. G., Vilhu O., Hassall B. J. M., Kellett B. J., Mason K. O., Piirola V., 1993, MNRAS, 263, 61
Harrop-Allin M. K., 1999, PhD Thesis, University of London
Harrop-Allin M. K., Cropper M., Hakala P. J., Hellier C., Ramseyer T., 1999, MNRAS, 308, 807 (Paper 2)
Harrop-Allin M. K., Hakala P. J., Cropper M., 1998, MNRAS, 302, 362 (Paper 1)
Heerlein C., Horne K., Schwope A. D., 1999, MNRAS, 304, 145
King A. R., Cannizzo J. W., 1998, ApJ, 499, 348
Kube, J., Gaensicke, B. T., Beuermann, K., 2000, A&A, 356, 490
Liebert J., Stockman H. S., 1985, in Lamb D.Q., Patterson J., eds, Proc. 7th North American Workshop on Cataclysmic Variables and Low Mass X-ray Binaries. Reidl, Dordrecht, p. 151
Livio M., Pringle J.E., 1994, ApJ, 427, 956
Lubow S. H., Shu F. H., 1975, ApJ, 198, 383
Perryman M. A. C., Cropper M., Ramsay G., Favata F., Peacock A., Rando N., Reynolds A., 2001, MNRAS, in press
Potter S.B., Hakala P.J., Cropper M., 1998, MNRAS, 297, 1261
Schwope A.D., Mantel K.H., Horne K., 1997, A&A, 319, 894
Schwope A. D., Schwarz R., Staude A., Heerlein C., Horne K., Steeghs D., 1999, in Hellier, C., Mukai, K., eds, ASP Conf. Ser. 157, Proc Annapolis Workshop on Magnetic Cataclysmic Variables, Astron. Soc. Pac., San Francisco, p. 71
Schwope A. D., Schwarz R., Mantel K.-H., Horne K., Beuermann K., 1995, in Buckley D. A. H., Warner B., eds, Cape Workshop on magnetic cataclysmic variables, ASP Conf. Ser. no. 85. Astron. Soc. Pac., San Francisco, p. 166
Schwope A. D., Thomas H.C., Beuermann K., 1993, A&A, 271, 25
Schwope A. D. et al., 1998, in Howell S., Kuulkers E., Woodward C., eds, ASP Conf. Ser. 137, Proceedings of the 13th North American Workshop on CVs. Astron. Soc. Pac., San Francisco, p. 44
Vrielmann, S., Schwope, A. D., 1999, in Hellier, C., Mukai, K., eds, ASP Conf. Ser. 157, Proc Annapolis Workshop on Magnetic Cataclysmic Variables, Astron. Soc. Pac., San Francisco, p. 93
Warner B., 1995, Cataclysmic variable stars. Cambridge Univ. Press, Cambridge

Wickramasinghe D. T., Meggitt S. M. A., 1985, MNRAS, 214, 605